PHOTONICS Research

Femtosecond mid-IR optical vortex laser based on optical parametric chirped pulse amplification

Junyu Qian,[1,2] Yujie Peng,[1,3,4] Yanyan Li,[1] Pengfei Wang,[1,2] Beijie Shao,[1,2] Zhe Liu,[1] Yuxin Leng,[1,3,5] and Ruxin Li[1,3,6]

[1]State Key Laboratory of High Field Laser Physics, Shanghai Institute of Optics and Fine Mechanics, Chinese Academy of Sciences, Shanghai 201800, China
[2]Center of Materials Science and Optoelectronics Engineering, University of Chinese Academy of Sciences, Beijing 100049, China
[3]CAS Center for Excellence in Ultra-intense Laser Science, Shanghai 201800, China
[4]e-mail: yjpeng@siom.ac.cn
[5]e-mail: lengyuxin@mail.siom.ac.cn
[6]e-mail: ruxinli@mail.shcnc.ac.cn

Received 5 December 2019; revised 18 January 2020; accepted 21 January 2020; posted 23 January 2020 (Doc. ID 385190); published 28 February 2020

A femtosecond mid-infrared optical vortex laser can be used for high harmonic generation to extend cutoff energy to the kilo-electron-volt range with orbital angular momentum, as well as other secondary radiations. For these, we demonstrate a high-energy femtosecond 4 μm optical vortex laser based on optical parametric chirped pulse amplification (OPCPA) for the first time. The optical vortex seed is generated from a femtosecond 4 μm laser by a silicon spiral phase plate with the topological charge l of 1 before the stretcher. Through using a two-stage collinear OPCPA amplifier, the chirped vortex pulse is amplified to 12.4 mJ with 200 nm full width at half-maximum bandwidth. After compression, the vortex laser pulse with 9.53 mJ, 119 fs can be obtained. Furthermore, the vortex characteristics of the laser beam are investigated and evaluated. This demonstration can scale to generate a higher-peak-power vortex mid-IR laser and pave a new way for high field physics.

https://doi.org/10.1364/PRJ.385190

1. INTRODUCTION

An optical vortex [1–3] refers to a beam whose wavefront appears as a helical shape. Due to the helical variation of the phase along propagation, the beam has an undefined phase at the center, which varies from 0 to $2\pi l$ around the center of spot, where l is the topological charge. The main feature of the optical vortex is that during the forward propagation of the beam, the optical vortex carries orbital angular momentum (OAM) of $\pm l\hbar$ per photon. Compared to the conventional Gaussian beam, since the optical vortex has doughnut intensity distribution and OAM, it has acquired considerable interest in science and technology, including quantum information [4–6], optical trapping and manipulation [7], super-resolution microscopy [8,9], optical communication [10], and high-order harmonic generation (HHG) [11–13]. In particular, the mid-infrared (mid-IR) optical vortex has important applications in the research of HHG. Compared with the traditional HHG experiment, high-energy mid-IR optical vortex lasers driving HHG have unique advantages. Phase-matching plays a relevant role for the efficient production of XUV/soft X-ray harmonics; due to the involved transverse field structure of the optical vortex, transverse phase-matching is especially relevant in HHG driven by vortex beams [14]. At the same time, using an optical vortex to drive HHG can produce ultraviolet photons carrying OAM. And the HHG with OAM can provide one more means of diagnosis for applications, besides temporal, spatial, energy, and momentum resolution. On the other hand, since the cutoff energy of higher-harmonic radiation is proportional to the square of the laser wavelength, higher-energy photons can be obtained by using longer wavelengths. Therefore, using the mid-IR optical vortex to generate high-order harmonics to produce an optical vortex in shorter wavelength regions may also open up completely new research directions in the areas of optical physics and material characterization.

Spurred by these exciting technologies, widespread attention has been paid to the generation and manipulation of the optical vortex, such as to use the diffractive optical elements including q-plates, spiral phase plates (SPPs), and phase modulation equipment such as spatial light modulators to generate optical vortices. However, these methods have certain disadvantages, such as low conversion efficiency, low damage threshold, and wavelength limitation. Therefore, due to these factors, generating high-energy femtosecond optical vortices directly by the diffractive optical elements has many disadvantages.

Although optical vortices in the visible [15] and near-IR [16,17] regions have been extensively used in most research and applications, the high-energy femtosecond optical vortex in the mid-IR region has not been fully researched to date, for the difficulties of amplifying the optical vortices in this wavelength range.

In recent times, with the development of nonlinear frequency conversion, efforts have been made previously to generate longer-wavelength optical vortices through optical parametric amplifiers (OPAs) [18] and optical parametric oscillators [19–21]. However, producing the high-energy femtosecond optical vortices has also been a challenge. Optical parametric chirped pulse amplification (OPCPA) combines OPA and chirped pulse amplification (CPA) technologies, which has its unique advantages, such as high gain, high temporal contrast, less thermal effect, and tunable wavelength, and it has been widely employed in recent high-peak-power laser systems [22]. Therefore, OPCPA is able to be an effective technology to generate high-energy femtosecond mid-IR optical vortices.

In this paper, we demonstrate a high-energy femtosecond 4 μm optical vortex laser system. Using a two-stage OPCPA, the 4 μm optical vortex laser beams generated by an SPP are amplified. A 4 μm optical vortex laser with 20 Hz, 9.53 mJ, 119 fs, and a topological charge of 1 is obtained. This high-energy 4 μm optical vortex laser source provides a new tool in the area of high field laser physics and can suit as a driver laser for HHG to extend the cutoff energy to kilo-electron-volt range with OAM, as well as other secondary radiations. Further, it is demonstrated that the higher-energy femtosecond optical vortex laser pulse can be obtained by the OPCPA method.

2. EXPERIMENT SETUP

The schematic of the 4 μm optical vortex laser system is presented in Fig. 1. The system consists of a 1 kHz Ti:sapphire CPA (Astrella, Coherent Inc.), a home-built 4 μm OPA device [23], a 4 μm SPP for vortex generation, a specially designed Nd:YAG picosecond pump laser (EKSPLA, Lithuania), and a two-stage OPCPA preceded by a conventional Öffner-type stretcher and followed by a two-grating compressor.

In the system, the Ti:sapphire femtosecond laser provides a laser of 3 mJ, 36 fs at 800 nm with a repetition rate of 1 kHz as a driving source. The 800 nm laser pulse passes through a home-built 4 μm OPA device to generate the seed pulse with 82 μJ energy.

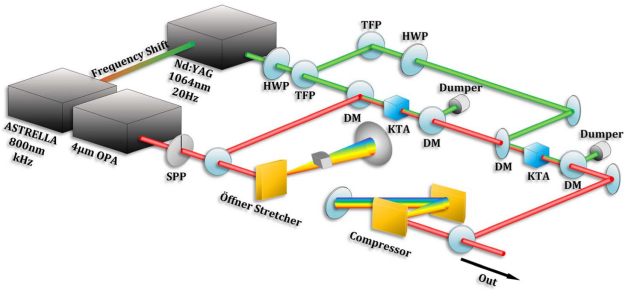

Fig. 1. Schematic of the 4 μm optical vortex OPCPA system. SPP, spiral phase plate; HWP, half-wave plate; TFP, thin film polarizer; DM, dichroic mirror; KTA, $KTiOAsO_4$.

The 4 μm pulse is delivered onto an SPP, and it is converted into an optical vortex with 36 μJ energy and a topological charge l of 1. The SPP is made of silicon with the step height of 1650 nm, and its thickness is 400 μm. The refractive index of silicon at 4 μm is 3.4258, and therefore the 1650 nm step height corresponds to the 2π phase variation. The surface shape of the SPP is continuous, so the phase variation of the optical vortex is also continuous.

Then, an Öffner stretcher based on a 300 grooves/mm gold-coated grating is employed to stretch the vortex pulse duration to ~70 ps. The efficiency of the Öffner stretcher is 55.6%, so the stretched pulse with 20 μJ is used as the signal light injection of the following OPCPA. The pump laser for the OPCPA is a commercial 1064 nm Nd:YAG laser with up to 250 mJ energy, a pulse duration of 70 ps, and a repetition rate of 20 Hz. In order to solve the problem of time synchronization between the pump and kilohertz femtosecond laser, the seed of the pump laser is from the oscillator of the kilohertz laser by a wavelength shifter.

After the stretcher, the chirped vortex is injected into the OPCPA amplifier. The pump laser is split into two beams of 30 mJ and 180 mJ, which are respectively transmitted onto the first and second crystals by image relaying. Since there is good transparency and nonlinear optical properties in the mid-IR region, two $KTiOAsO_4$ (KTA) crystals are used in the OPAs, which both have 10 mm length and are cut at $\theta = 40.8°$ relative to the z-axis normal for Type II phase-matching. The relative delay of the signal and pump pulses can be adjusted by a delay line. After the first stage, the energy of the 4 μm signal pulse is amplified to 1.14 mJ and after the second stage, the 4 μm optical vortex pulse is further amplified to 12.4 mJ.

Then, the pulse with 12.4 mJ energy after the second OPA stage is sent into a two-grating compressor. The compressor is designed to match the stretcher, for precise dispersion compensation. After being compressed by the two-grating compressor, the pulse width of the amplified optical vortex is 119 fs and the energy can be up to 9.53 mJ.

3. EXPERIMENT RESULTS AND DISCUSSION

After successfully amplifying the vortex beam, we have measured the energy scaling characteristics of the OPCPA. The pump energy of the first-stage OPA is 30 mJ, so that the amplified signal energy is 1.14 mJ. The gain in the second-stage high-energy OPA is described as a function of the signal and the pump energies in Fig. 2. It shows that the second amplified signal energy has a linear growth relationship with the increasing of pump energy. It also shows that the amplified energy of the second stage has not reached saturation yet when pumped by 180 mJ. The pump spot diameter of the second OPA is 6 mm, that is, the energy density is 637 mJ/cm^2, which is close to the damage threshold of the optical elements in our system. Therefore, the 4 μm optical vortex is amplified to a maximum of 12.4 mJ in the second OPA stage. Of course, if using a larger KTA crystal and higher pump energy, a higher conversion efficiency and output energy can be obtained. One of the advantages of OPCPA is less thermal effect, and KTA is a temperature-insensitive nonlinear crystal which has a very high thermal acceptance. With an efficient heat dissipation

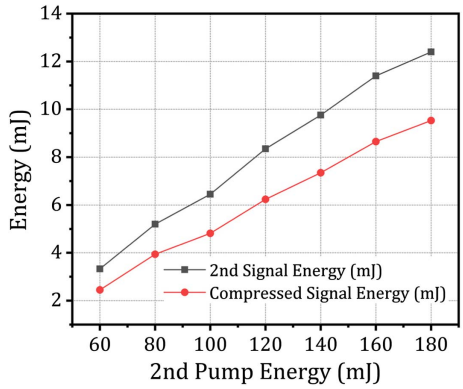

Fig. 2. Amplified signal pulse energy after the second-stage OPA and compressor as a function of the second pump energy.

condition, the OPCPA system can support kilowatt-level working condition.

The efficiency of the compressor is 76.9%, and the inherent diffraction efficiency of a single grating is about 94%. After being compressed by the two-grating compressor, the maximum output energy of the optical vortex is 9.53 mJ.

To verify the generation of the optical vortex, the intensity distribution of the signal laser is measured using a pyroelectric array CCD camera (Spiricon Pyrocam IV) with the pixel size of 80 μm × 80 μm, and the result is shown in Fig. 3(a). It can be seen that the beam profile exhibits a doughnut intensity distribution after passing through the SPP as expected, but the intensity distribution is a little uneven due to the low transmittance at the step of the SPP. At the same time, due to the inherent dispersion characteristic of the silicon SPP and 200 nm full width at half-maximum (FWHM) of the emission spectrum of the OPA, when the femtosecond pulse passes through the SPP, the phase differences generated by different wavelength components are different, resulting in the deviation of the topological charge and affecting the quality of the optical vortex to a certain extent.

To investigate the wavefront of the optical vortex, we used a 30:70 beam splitter to split a part of the pulse produced by the 4 μm OPA. This part of the plane pulse interfered with the vortex pulse generated by the SPP at the far field, and the interference fringes are shown in Fig. 3(b). As can be seen from the figure, the central bright stripe shows a pair of Y-shaped fringes at the phase singularity (circled by the dotted blue line), which also demonstrates that the pulse is a first-order optical vortex.

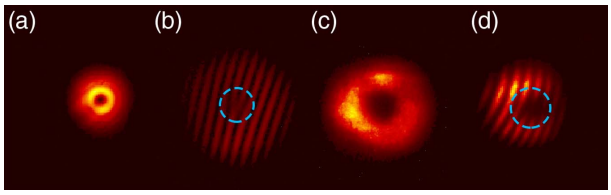

Fig. 3. (a) Spatial profile of the 4 μm vortex output after SPP. (b) Interference fringes of vortex and plane beams. (c) Spatial profile of the amplified 4 μm vortex output. (d) Interference fringes of amplified vortex and plane beams.

The spatial profile of the compressed optical vortex is shown in Fig. 3(c), which indicates that the intensity still maintains a good doughnut shape. And it can be seen from the figure that the intensity of the spot after the OPCPA is slightly uneven, which is because during the amplification, the unevenness of the spot after the SPP is further enlarged.

In order to obtain the interference image of the compressed vortex and plane light, we divided the compressed vortex into two beams; one is the vortex beam, and the other vortex beam is expanded and intercepted to obtain a small portion of the light spot, which can be approximated as plane light. The two beams interfere in the far field, and the resulting interference fringes are as shown in Fig. 3(d). It can be seen that the central bright stripe branches into two (circled by the dotted blue line), indicating that the compressed light still maintains a good vortex characteristic and the topological charge is still 1. The bending of the interference fringes is due to the fact that the plane wave is a small part intercepted from the vortex beam, so the wavefront is not completely planar.

To maintain the vortex quality, the beam amplification and propagation should be well controlled. First, although the OPCPA process does not affect the spatial phase, the pump laser should be a flat-top distribution to ensure that each part of the vortex beam can be amplified equally without destroying the vortex structure. Second, the mirrors and lenses used in the system should be with good surface, which can keep the wavefront of the vortex beam.

We also measured the spectral characteristics of the optical vortex by an acousto-optic-based scanning spectrometer (MOZZA, Fastlite). Figure 4 shows the spectra for four segments of the beam selected from different quadrants of the doughnut. The spectra of all four parts have almost the same bandwidths, ~200 nm FWHM, and spectral shapes. The slight inconsistency of the spectra in Fig. 4 is mainly due to the slight unevenness in the amplification process and the unevenness of the 4 μm OPA seed source spectrum. But these are very small effects, and the spatial chirp is basically negligible.

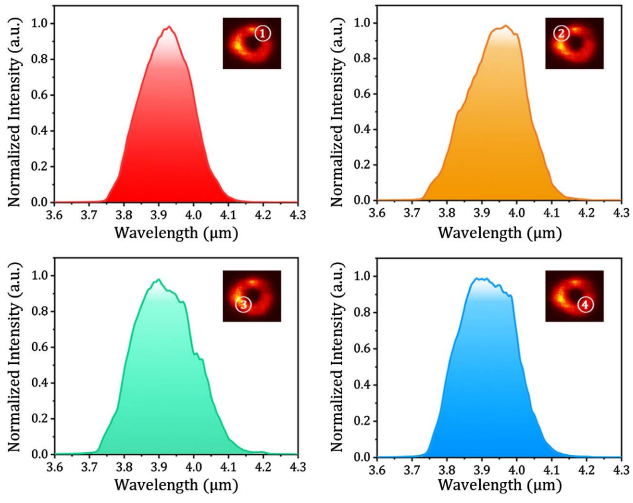

Fig. 4. Spectra of the optical vortex beam measured at four different quadrants after the compressor. The small figures and the serial numbers show the measured position of the spot.

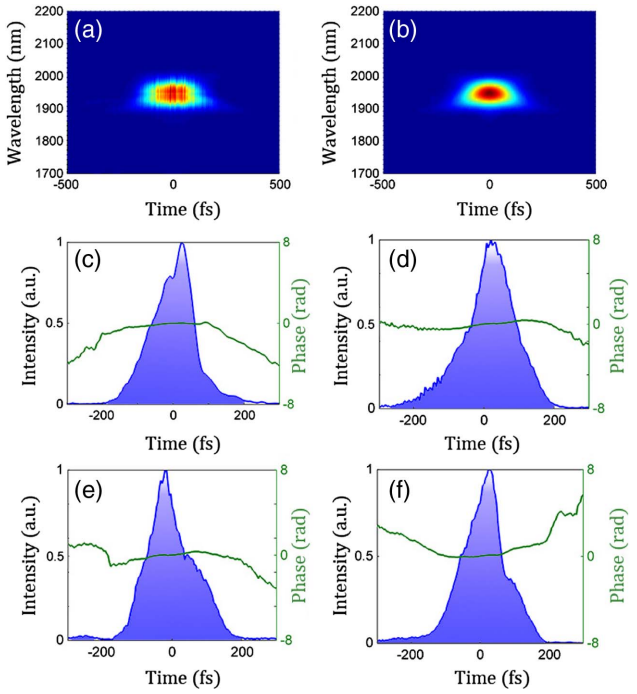

Fig. 5. (a) Measured and (b) reconstructed SHG-FROG traces. (c)–(f) Temporal profiles of the optical vortex beam measured at first to fourth quadrants.

Temporal characterization of the vortex pulse is measured by a home-built second-harmonic-generation frequency-resolved optical gating (SHG-FROG) setup [24] employing a 200 μm $AgGaS_2$ crystal. By optimizing the grating angles and separation distance of the gratings in the compressor, we measured the pulse width of the first quadrant of the beam with a minimum pulse width of 119 fs, which is close to the Fourier-transform-limited duration of 116 fs. Temporal characterizations of the OPCPA output pulse measured and retrieved from the SHG-FROG measurement results are shown in Fig. 5.

Figures 5(a)–5(c) show the temporal characterizations of the first quadrant of the optical vortex. Figures 5(a) and 5(b) respectively represent the measured and retrieved traces by the SHG-FROG. Figure 5(c) shows the reconstructed pulse in blue and phase in green, which indicates the compressed pulse duration is 119 fs. The temporal profiles of the other three different quadrants of the compressed pulse are shown in Figures 5(d)–5(f). These curves correspond to 127 fs, 116 fs, and 119 fs for these three parts. The errors of the FROG inversion are about 0.4%. Therefore, in the time domain, the different parts of the beam also have good consistency.

4. CONCLUSION

In conclusion, we report a high-energy femtosecond 4 μm optical vortex laser system based on OPCPA. The pulse emitted by the 4 μm OPA is converted into an optical vortex by an SPP. Then, the vortex pulse is introduced as a signal pulse into the two-stage collinear KTA OPCPA to be amplified. A laser with 9.53 mJ, 119 fs, 20 Hz optical vortex is obtained finally. By interfering with the plane wave, we verified that its topological charge is 1. Moreover, the optical vortex amplified by OPCPA can still maintain good vortex characteristics. This high-energy, mid-IR optical vortex laser source is highly suitable for driving various nonlinear optical phenomena, such as HHG and high-flux coherent extreme ultraviolet or soft X-ray radiation. Moreover, this method can be further extended to optical vortex lasers with other wavelengths and higher peak power.

Funding. Strategic Priority Research Program of the Chinese Academy of Sciences (XDB1603); International ST Cooperation Program of China (2016YFE0119300); Program of Shanghai Academic/Technology Research Leader (18XD1404200); Shanghai Municipal Science and Technology Major Project (2017SHZDZX02); National Natural Science Foundation of China (11127901, 61925507).

Disclosures. The authors declare no conflicts of interest.

REFERENCES

1. L. Allen, M. W. Beijersbergen, R. J. Spreeuw, and J. P. Woerdman, "Orbital angular momentum of light and the transformation of Laguerre–Gaussian laser modes," Phys. Rev. A **45**, 8185–8189 (1992).
2. G. Indebetouw, "Optical vortices and their propagation," J. Mod. Opt. **40**, 73–87 (1993).
3. M. S. Soskin and M. V. Vasnetsov, "Singular optics," Prog. Opt. **42**, 219–276 (2001).
4. R. Inoue, T. Yonehara, Y. Miyamoto, M. Koashi, and M. Kozuma, "Measuring qutrit-qutrit entanglement of orbital angular momentum states of an atomic ensemble and a photon," Phys. Rev. Lett. **103**, 110503 (2009).
5. A. Mair, A. Vaziri, G. Weihs, and A. Zeilinger, "Entanglement of the orbital angular momentum states of photons," Nature **412**, 313–316 (2001).
6. G. Molina-Terriza, J. P. Torres, and L. Torner, "Twisted photons," Nat. Phys. **3**, 305–310 (2007).
7. A. M. Yao and M. J. Padgett, "Orbital angular momentum: origins, behavior and applications," Adv. Opt. Photon. **3**, 161–204 (2011).
8. S. Bretschneider, C. Eggeling, and S. W. Hell, "Breaking the diffraction barrier in fluorescence microscopy by optical shelving," Phys. Rev. Lett. **98**, 218103 (2007).
9. T. Watanabe, Y. Iketaki, T. Omatsu, K. Yamamoto, S. Ishiuchi, M. Sakai, and M. Fujii, "Two-color far-field super-resolution microscope using a doughnut beam," Chem. Phys. Lett. **371**, 634–639 (2003).
10. Y. Yan, G. Xie, M. P. Lavery, H. Huang, N. Ahmed, C. Bao, Y. Ren, Y. Cao, L. Li, Z. Zhao, A. F. Molisch, M. Tur, M. J. Padgett, and A. E. Willner, "High-capacity millimetre-wave communications with orbital angular momentum multiplexing," Nat. Commun. **5**, 4876 (2014).
11. C. Hernandez-Garcia, A. Picon, J. San Roman, and L. Plaja, "Attosecond extreme ultraviolet vortices from high-order harmonic generation," Phys. Rev. Lett. **111**, 083602 (2013).
12. D. Gauthier, P. R. Ribic, G. Adhikary, A. Camper, C. Chappuis, R. Cucini, L. F. DiMauro, G. Dovillaire, F. Frassetto, R. Geneaux, P. Miotti, L. Poletto, B. Ressel, C. Spezzani, M. Stupar, T. Ruchon, and G. De Ninno, "Tunable orbital angular momentum in high-harmonic generation," Nat. Commun. **8**, 14971 (2017).
13. L. Rego, K. M. Dorney, N. J. Brooks, Q. L. Nguyen, C. T. Liao, J. San Roman, D. E. Couch, A. Liu, E. Pisanty, M. Lewenstein, L. Plaja, H. C. Kapteyn, M. M. Murnane, and C. Hernandez-Garcia, "Generation of extreme-ultraviolet beams with time-varying orbital angular momentum," Science **364**, eaaw9486 (2019).
14. C. Hernandez-Garcia, L. Rego, J. San Roman, A. Picon, and L. Plaja, "Attosecond twisted beams from high-order harmonic generation driven by optical vortices," High Power Laser Sci. Eng. **5**, e3 (2017).
15. M. Koyama, A. Shimomura, K. Miyamoto, and T. Omatsu, "Frequency-doubling of an optical vortex output from a stressed Yb-doped fiber amplifier," Appl. Phys. B **116**, 249–254 (2014).

16. Y. F. Chen and Y. P. Lan, "Dynamics of the Laguerre Gaussian $TEM_{0,1}^{*}$ mode in a solid-state laser," Phys. Rev. A **63**, 063807 (2001).
17. J. W. Kim, J. I. Mackenzie, J. R. Hayes, and W. A. Clarkson, "High power Er:YAG laser with radially-polarized Laguerre-Gaussian (LG_{01}) mode output," Opt. Express **19**, 14526–14531 (2011).
18. A. Aadhi and G. K. Samanta, "High-power, high repetition rate, tunable, ultrafast vortex beam in the near-infrared," J. Opt. **20**, 01LT01 (2018).
19. A. Aadhi, V. Sharma, R. P. Singh, and G. K. Samanta, "Continuous-wave, singly resonant parametric oscillator-based mid-infrared optical vortex source," Opt. Lett. **42**, 3674–3677 (2017).
20. K. Miyamoto, S. Miyagi, M. Yamada, K. Furuki, N. Aoki, M. Okida, and T. Omatsu, "Optical vortex pumped mid-infrared optical parametric oscillator," Opt. Express **19**, 12220–12226 (2011).
21. A. Smith and D. Armstrong, "Generation of vortex beams by an image-rotating optical parametric oscillator," Opt. Express **11**, 868–873 (2003).
22. P. Wang, Y. Li, W. Li, H. Su, B. Shao, S. Li, C. Wang, D. Wang, R. Zhao, Y. Peng, Y. Leng, R. Li, and Z. Xu, "2.6 mJ/100 Hz CEP-stable near-single-cycle 4 μm laser based on OPCPA and hollow-core fiber compression," Opt. Lett. **43**, 2197–2200 (2018).
23. Y. Chen, Y. Y. Li, W. K. Li, X. Y. Guo, and Y. X. Leng, "Generation of high beam quality, high-energy and broadband tunable mid-infrared pulse from a KTA optical parametric amplifier," Opt. Commun. **365**, 7–13 (2016).
24. Y. Li, Y. Chen, W. Li, P. Wang, B. Shao, Y. Peng, and Y. Leng, "Accurate characterization of mid-infrared ultrashort pulse based on second-harmonic-generation frequency-resolved optical gating," Opt. Laser Technol. **120**, 105671 (2019).